EAI Endorsed Transactions
on Industrial Networks and Intelligent Systems
Research Article EAI.EU

Jamming for Security in Cognitive NOMA with Full-Duplex Energy Scavenging Unlicensed Transmitter

Hoan Tran[1,2], Khuong Ho-Van[1,*], Pham Ngoc Son[2]

[1]Ho Chi Minh City University of Industry and Trade, Ho Chi Minh City, Vietnam
[2]Ho Chi Minh City University of Technology and Engineering, Ho Chi Minh City, Vietnam

Abstract

The combination of non-orthogonal multiple access (NOMA), cognitive radio (CR), energy scavenging (ES), and full-duplex (FD) transmission significantly improves spectral efficiency, spectrum utilization, and energy efficiency - key performance indicators in the development of future wireless communications infrastructures. Nonetheless, the growing threat of eavesdropping necessitates robust physical-layer security mechanisms. The paper proposes NOMA CR networks with FD ES unlicensed transmitter (UT), referred to as NOEHwJ, to exploit primary interference as an energy source for UT's operation and a jamming source to secure UT's information. An in-depth evaluation of reliability and secrecy metrics for NOEHwJ is also presented. Through rigorous theoretical analysis and simulation, the study elucidates the impact of each enabling technology on secrecy capability. It is evident from the results that NOEHwJ delivers marked enhancements in security when compared to the benchmarked orthogonal multiple access (OMA) CR networks with FD ES UT (OEHwJ), thereby demonstrating the superior advantages of jointly employing CR, ES, NOMA, FD, and jamming techniques for the development of wireless communication architectures that are secure, energy-efficient, and adaptable to future demands.

Received on 17 March 2026; accepted on 13 April 2026; published on 21 April 2026

Keywords: NOMA; energy scavenging; cognitive radio; full-duplex; jamming.

doi:10.4108/eetinis.131.12260

1. Introduction

1.1. General context

As wireless communication paradigms evolve from 5G to 6G, they are expected to support an expansive array of emerging applications, driven by the need to accommodate increasingly stringent communication requirements for a vast network of connected devices [1, 2]. Although these systems are designed to enable high-speed transmission with extremely low delay, challenges remain in power and bandwidth allocation, especially when the quantity of devices continues to grow. Ensuring secure and reliable communications also emerges as a critical issue that system designers must address. Thus, optimizing both energy and spectrum efficiency alongside communication security and reliability remains a critical design goal.

The synergy between CR and NOMA technologies provides an effective solution for improving spectrum utilization in modern wireless communication systems [3–5]. More specifically, NOMA enables multiple users to communicate simultaneously [6], while CR facilitates flexible spectrum access, allowing secondary users to operate alongside primary users. Furthermore, NOMA supports wireless energy harvesting from ambient sources, thereby enhancing energy efficiency - an increasingly important trend in line with the evolution of ES technologies in 5G and 6G [7, 8]. In addition, FD communication enhances spectral efficiency by allowing concurrent transmission and reception over identical system resources [9], unlike half-duplex (HD) systems, which perform these operations in a time- or frequency-separated manner. However,

*Corresponding author. Email: khuonghv@huit.edu.vn

the increasing sophistication of eavesdropping attacks has underscored the need for robust physical-layer security mechanisms. Among the emerging security solutions, jamming - deliberate interference to degrade the eavesdroppers' reception quality - has shown considerable promise in reinforcing system security [10–13]. The integration of CR, NOMA, FD, ES, and jamming forms NOFEwJ, which holds great potential for enhancing reliability, security, capacity, and energy efficiency in modern wireless communication networks.

1.2. Related works

A communication model that integrates NOMA, CR and FD was recommended in [14] to meliorate spectral efficiency and enable simultaneous transmission. However, the absence of ES renders the system entirely dependent on external power sources, which undermines sustainability and energy autonomy - especially for devices deployed in remote or hard-to-reach environments. Furthermore, the lack of jamming mechanisms compromises the security of the system against potential wire-tapping problems.

The study in [15] incorporates ES and jamming into a NOMA-based communication model, but excludes CR and FD capabilities. While jamming enhances security and ES improves energy self-sufficiency, the lack of CR reduces spectral adaptability, and the absence of FD prevents simultaneous information reception and transmission. Consequently, the system exhibits limitations in both spectral efficiency and transmission capacity.

Security issues in CR-enabled networks integrated with ES and NOMA have been addressed in the studies [16–25]. Although these models offer relatively simple designs, they suffer from critical limitations in terms of both security and system throughput. The omission of jamming diminishes resilience to eavesdropping, while the lack of FD capability hinders concurrent data and ES operations, thus reducing overall system efficiency.

Alternatively, communication models that combine NOMA, FD, and ES to ameliorate energy and spectral efficiency in wireless networks have been proposed in [26–30]. Nevertheless, CR plays a pivotal role in exploiting underutilized spectrum from primary networks but excluding CR in [26–30] significantly restricts the system's spectral efficiency. Additionally, the absence of jamming mechanisms not only weakens the system's security but also results in suboptimal spectrum utilization.

Communication models presented in [3] and [31] integrate technologies (NOMA, CR, ES, jamming) into a unified framework. However, the exclusion of FD impairs the system's ability to perform simultaneous transmission and reception, which negatively impacts latency and spectral performance. On the other hand, this simplification avoids self-interference and reduces signal processing complexity.

Similarly, communication models proposed in [32–34] incorporate technologies (NOMA, ES, FD, jamming), but do not consider the CR environment. These studies evaluate several key performance indicators, such as coverage/information energy efficiency (CEE/IEE), coverage/information outage probability (COP/IOP), and information/correct transmission probability (ITP/CTP). However, the analyses do not exploit the benefits of spectrum sharing in CR settings, leading to inefficient spectrum utilization.

The work in [35] advances the literature by proposing a NOMA-based system that includes CR and FD. Notwithstanding, the lack of ES deteriorates energy efficiency. Also, the absence of jamming mechanisms induces the system to be vulnerable to wire-tapping, particularly in wireless environments where adversaries may be present. This emphasizes the important role of ES and jamming in ameliorating privacy and energy efficiency for NOMA CR networks with FD operation.

In summary, current researches have yet fully addressed the security challenges in NOMA CR networks with FD ES UT to exploit primary interference as an energy source for UT's operation and a jamming source to secure UT's information. This paper bridges this gap by proposing a novel framework, referred to as NOFEwJ, along with an analytical model to facilitate rapid optimization and evaluation of system performance prior to practical deployment.

1.3. Contributions

The principal contributions and insights presented in this paper are as follows:

- An advanced wireless communication structure, denoted as NOFEwJ, is developed by integrating NOMA, FD transmission, and ES within a CR framework. The system architecture is optimized to boost spectral utilization and energy performance in tandem, catering to the requirements of advanced wireless networks.

- A thorough performance assessment is conducted in terms of key indicators, including reliable and secrecy throughput (RST/SST), reliable and secrecy outage probability (ROP/SOP), and reliable and secrecy energy efficiency (REE/SEE). The analysis accounts for realistic operational scenarios and reveals the significant roles of ES, NOMA, jamming, and FD in influencing system performance.

- Comparative analysis demonstrates that NOFEwJ achieves superior secrecy performance relative

to a benchmarked OMA CR networks with FD ES UT, thus underscoring the superiorities of synergistically integrating NOMA and FD techniques for secure and efficient wireless communication.

1.4. Paper organizaton

The next section presents the proposed system model (NOFEwJ). Following that, Section 3 delivers a thorough evaluation of the system's performance based on critical assessment metrics, including RST, SST, REE, SEE, as well as ROP and SOP. Section 4 presents a performance analysis of the benchmark scheme (OFEwJ), which is based on OMA and operates under the same conditions as NOFEwJ. This comparison aims to assess the security impact of incorporating NOMA into the FD scenario. Section 5 discusses the simulation and analytical results obtained under various practical scenarios to comprehensively assess and compare the system performance. Eventually, Section 6 summarizes the crucial insights and findings derived from the study. All detailed derivations are moved to Appendices. Also, symbols frequently used are listed in Table 1.

Table 1. Frequently-used symbols

Symbol	Description
t	Transmit signal at UT
ϕ	Power fraction for the transmission of t_d
P_u	Transmission power of UT
t_d/t_c	Transmit signal intended for DU/CU
$\Xi\{\cdot\}$	Expectation operator
k_{zm}	Channel fading coefficient
b_{zm}	Channel power gain
h_{zm}	Fading power
α	Path-loss decay
k_{uu}	Fading coefficient of the loopback channel
P_t	Transmission power of LT
t_t	Transmit signal by LT
$\tilde{P}_u$	Energy harvested at UT
φ	Energy harvesting efficiency
Q	Maximum interference power
N_0	Normalized noise power
E	Predefined spectral efficiency
Λ_d^d/Λ_c^c	ROP of DU/CU
$\Pr\{\cdot\}$	Probability operator
κ	Successful decoding threshold in NOFEwJ
$\overline{\kappa}$	Successful decoding threshold in OFEwJ

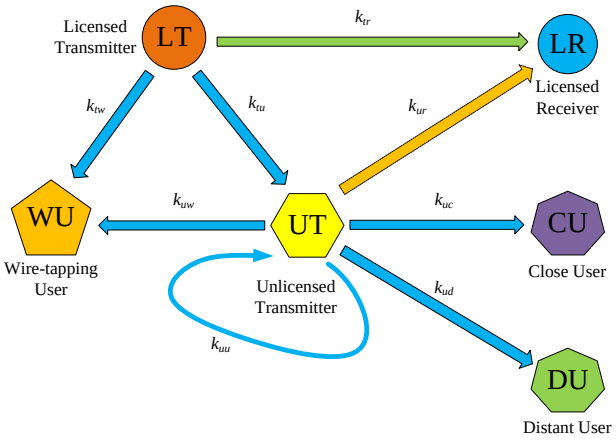

Figure 1. NOMA CRNs with FD ES UT

2. NOMA CRNs with FD ES UT

The proposed NOFEwJ is demonstrated in Fig. 1 and comprises the components: licensed transmitter (LT), unlicensed transmitter (UT), licensed receiver (LR), distant NOMA user (DU), close NOMA user (CU), and wire-tapping user (WU). This system model may be designed for application in downlink communication scenarios within wireless networks. UT, being energy-limited, relies on harvesting energy from LT. LT can be a dedicated energy transmitter, such as broadcast radio or television stations. In this model, UT operates in FD mode, which enables it to simultaneously harvest energy from LT while performing NOMA transmission to DU and CU, and concurrently causing interference to LR. UT broadcasts, in particular, a composite signal denoted by $t = \sqrt{\phi P_u} t_d + \sqrt{(1-\phi) P_u} t_c$. In the expression of t, ϕ denotes the power distribution coefficient for the transmission of t_d; P_u represents the transmit power at UT; t_d and t_c are the information-bearing signals intended for DU and CU, respectively, with $\Xi\left\{|t_l|^2\right\} = 1$, $l = \{c, d\}$, and $\Xi\{\cdot\}$ denoting the expectation operator. According to the NOMA protocol, t_c is transmitted with lower power compared to t_d. Therefore, the parameter is configured such that $\phi > 0.5$, ensuring compliance with NOMA's power-domain multiplexing principle. Furthermore, owing to the broadcast characteristic inherent in wireless communications, transmissions from UT are vulnerable to interception by WU. In order to protect the secrecy of UT's transmissions, LT concurrently operates as a cooperative jammer, enhancing physical layer security by disrupting the wire-tapping user's signal reception.

Fig. 1 illustrates k_{zm}, where $zm = \{tw, tu, tr, ur, uw, ud, uc\}$ denotes the channel fading coefficient. This study assumes that all transmission links are independent and experience Rayleigh fading with flat block characteristics. The channel power gain

$b_{zm} = |k_{zm}|^2$ is thus modeled through its corresponding CDF[1] and probability density function (PDF), which are correspondingly addressed to be [36]

$$F_{b_{zm}}(q) = 1 - e^{-\frac{q}{h_{zm}}}, \tag{1}$$

$$f_{b_{zm}}(q) = \frac{e^{-\frac{q}{h_{zm}}}}{h_{zm}}. \tag{2}$$

Specifically, $h_{zm} = \Xi\{b_{zm}\}$ represents the average power loss, defined as the statistical average of the squared magnitude of the channel fading coefficient k_{zm}. In this study, h_{zm} is modeled as $h_{zm} = \beta d_{zm}^{-\alpha}$ to capture the path loss effect, with α being the path-loss decay, β indicating the path-loss coefficient at 1 meter, and d_{zm} representing the transmitter-receiver separation [37].

Moreover, due to its full-duplex capability, UT encounters self-interference (SI) while transmitting and receiving concurrently. As illustrated in Fig. 1, SI is modeled through a loopback channel with an associated fading coefficient k_{uu}. This parameter is assumed to follow a Rayleigh distribution [36], i.e., $k_{uu} \sim \mathcal{CN}(0, h_{uu})$, and its PDF is given by $f_{b_{uu}}(q) = \frac{e^{-\frac{q}{h_{uu}}}}{h_{uu}}$.

Due to its full-duplex operation, UT not only receives signals from LT but is also affected by SI caused by its own transmitted signal. Thus, the expression for the received signal at UT is

$$m_u = k_{tu}\sqrt{P_t}t_t + k_{uu}\sqrt{P_u}t + \zeta_u, \tag{3}$$

where P_t is LT's transmit power, t_t is the transmitted information signal with unit power such that $\Xi\left\{|t_t|^2\right\} = 1$ and $\zeta_u \sim \mathcal{CN}(0, N_u)$ models UT's noise. Because noise power is considerably lower than the received signal power, an approximation of the energy harvested at UT is given by $\tilde{P}_u \approx \varphi\left(b_{tu}P_t + b_{uu}\tilde{P}_u\right)$, which is equivalent to

$$\tilde{P}_u \approx \frac{\varphi b_{tu}}{1 - \varphi b_{uu}}P_t, \tag{4}$$

with $\varphi \in (0, 1)$ indicating the energy harvesting efficiency, and $b_{uu} < \frac{1}{\varphi}$.

Let Q denote the maximum permissible interference power at LR. For CRNs, UT's transmit power, denoted as P_u, is constrained by two factors: the maximum permissible transmit power $\tilde{P}_u$ and the interference threshold Q imposed at LR. To ensure both regulatory compliance and effective communication over the widest possible range, the transmit power is determined by the lesser of these two bounds, and can be mathematically expressed as [3]

$$P_u = \min\left(\tilde{P}_u, \frac{Q}{b_{ur}}\right). \tag{5}$$

UT transmits the NOMA signal t with the power P_u. At LU = {DU, CU}, the received signal is represented by

$$m_l = k_{ul}\sqrt{\phi P_u}t_d + k_{ul}\sqrt{(1-\phi)P_u}t_c + \zeta_l, \tag{6}$$

wherein $\zeta_l \sim \mathcal{CN}(0, N_l)$ denotes additive noise at LU. For analytical convenience, noise power is normalized such that $N_l = N_0$.

LU decodes its intended message by employing the successive interference cancellation (SIC) inherent in NOMA systems. Since $\phi > 0.5$, DU directly decodes t_d from $m_d = k_{ud}\sqrt{\phi P_u}t_d + k_{ud}\sqrt{(1-\phi)P_u}t_c + \zeta_d$ without the prerequisite of decoding t_c. Hence, SINR[2] experienced at DU when recovering t_d is derived as

$$\Psi_d^d = \frac{\phi P_u b_{ud}}{(1-\phi)P_u b_{ud} + N_0}. \tag{7}$$

Since $\phi > 0.5$, CU decodes t_d by treating t_c as interference. After successfully decoding and canceling t_d (i.e., interference from t_d is left), it proceeds to decode its intended signal t_c. Therefore, the SINR at CU for decoding t_d is

$$\Psi_c^d = \frac{\phi P_u b_{uc}}{(1-\phi)P_u b_{uc} + N_0}. \tag{8}$$

In a similar manner, signal-to-noise ratio (SNR) at CU corresponding to the decoding of t_c is given by

$$\Psi_c^c = \frac{(1-\phi)P_u b_{uc}}{N_0}. \tag{9}$$

WU receives a signal, which originates from UT but is jammed by LT. The signal is expressed as

$$m_w = k_{uw}\sqrt{\phi P_u}t_d + k_{uw}\sqrt{(1-\phi)P_u}t_c + k_{tw}\sqrt{P_t}t_t + \zeta_w, \tag{10}$$

wherein $\zeta_w \sim \mathcal{CN}(0, N_w)$ is WU's noise. For analytical convenience, the noise power N_w is normalized to N_0. WU first attempts to decode t_d by treating t_c as interference, and then cancels the interference from t_d before decoding t_c. Thus, the SINR at WU for decoding t_d is

$$\Psi_w^d = \frac{\phi P_u b_{uw}}{(1-\phi)P_u b_{uw} + P_t b_{tw} + N_0}. \tag{11}$$

Meanwhile, the SNR at WU for decoding t_c is expressed as

$$\Psi_w^c = \frac{(1-\phi)P_u b_{uw}}{P_t b_{tw} + N_0}. \tag{12}$$

Both (11) and (12) expose that the jamming power $P_t b_{tw}$ created by LT interrupts the signal reception of WU, leading to the enhanced security for DU and CU.

[1] CDF implies cumulative distribution function.

[2] SINR implies signal-to-interference plus noise ratio.

3. Analytical Evaluation of NOFEwJ

This section delivers an in-depth examination of NOFEwJ's performance in terms of security and reliability. Specifically, it begins with the derivation of SOP/ROP, which quantifies the likelihood that channel capacity at WU/LU, respectively, falls short of a predefined spectral efficiency requirement E.

Following this, the analysis proceeds with the evaluation of RST/SST and REE/SEE. These metrics comprehensively reflect the system's capability to ensure both secure communication and reliable data transmission, offering a holistic view of its performance across confidentiality and reliability dimensions.

3.1. ROP of DU

The ROP of DU, Λ_d^d, which is the probability that DU cannot decode t_d. Equivalently, the actual channel capacity at DU for restoring t_d is smaller than E:

$$\Lambda_d^d = \Pr\left\{\log_2\left(1+\Psi_d^d\right) \le E\right\} = \Pr\left\{\Psi_d^d < \kappa\right\}, \tag{13}$$

where $\kappa = 2^E - 1$.

Substituting (7) into (13) yields

$$\begin{aligned}\Lambda_d^d &= \Pr\left\{\frac{\phi P_u b_{ud}}{(1-\phi)P_u b_{ud} + N_0} < \kappa\right\} \\ &= \begin{cases} \Pr\left\{b_{ud} < \frac{N_0\kappa}{(\phi-[1-\phi]\kappa)P_u}\right\} & ,\kappa < \frac{\phi}{1-\phi} \\ 1 & ,\kappa \ge \frac{\phi}{1-\phi} \end{cases} \\ &= \begin{cases} \tilde{\Lambda}_d\left(Z_d\right) & ,\kappa < \frac{\phi}{1-\phi} \\ 1 & ,\kappa \ge \frac{\phi}{1-\phi} \end{cases}\end{aligned} \tag{14}$$

where $l = \{c, d\}$, $Z_d = \frac{N_0\kappa}{\phi-(1-\phi)\kappa}$, and

$$\tilde{\Lambda}_l(a) = \Pr\left\{b_{ul} < \frac{a}{P_u}\right\}, \tag{15}$$

which is deferred to Appendix A.

3.2. ROP of CU

The ROP of CU, denoted by Λ_c^c, is defined as the probability that CU either fails to decode t_d - that is, channel capacity for decoding t_d is less than E - or successfully decodes t_d but fails to decode t_c, meaning channel capacity for decoding t_c is also below E:

$$\begin{aligned}\Lambda_c^c &= \Pr\left\{\log_2\left(\Psi_c^d+1\right) < E\right\} \\ &\quad + \Pr\left\{\log_2\left(\Psi_c^d+1\right) \ge E, \log_2\left(\Psi_c^c+1\right) < E\right\} \\ &= \Pr\left\{\Psi_c^d < \kappa\right\} + \Pr\left\{\Psi_c^d \ge \psi, \Psi_c^c < \kappa\right\} \\ &= 1 - \Pr\left\{\Psi_c^d \ge \kappa, \Psi_c^c \ge \kappa\right\}.\end{aligned} \tag{16}$$

Substituting (8) and (9) into (16) yields

$$\begin{aligned}\Lambda_c^c &= 1 - \Pr\left\{\frac{\phi P_u b_{uc}}{(1-\phi)P_u b_{uc} + N_0} \ge \kappa, \frac{(1-\phi)P_u b_{uc}}{N_0} \ge \kappa\right\} \\ &= \begin{cases} 1-\Pr\left\{b_{uc} \ge \frac{N_0\kappa}{[\phi-\kappa(1-\phi)]P_u}, b_{uc} \ge \frac{N_0\kappa}{(1-\phi)P_u}\right\} & ,\kappa < \frac{\phi}{1-\phi} \\ 1 & ,\kappa \ge \frac{\phi}{1-\phi} \end{cases} \\ &= \begin{cases} \tilde{\Lambda}_c\left(Z_c\right) & ,\kappa < \frac{\phi}{1-\phi} \\ 1 & ,\kappa \ge \frac{\phi}{1-\phi} \end{cases}\end{aligned} \tag{17}$$

where $Z_c = \max\left(\frac{N_0\kappa}{\phi-\kappa(1-\phi)}, \frac{N_0\kappa}{1-\phi}\right)$.

3.3. SOP of WU

SOP for t_d. It is to evaluate the probability of WU failing to decode t_d from DU. This implies that channel capacity that WU can achieve for decoding t_d is smaller than E:

$$\Lambda_w^d = \Pr\left\{\log_2\left(1+\Psi_w^d\right) \le E\right\} = \Pr\left\{\Psi_w^d < \kappa\right\}. \tag{18}$$

Substituting (11) into (18) yields

$$\begin{aligned}\Lambda_w^d &= \Pr\left\{\frac{\phi P_u b_{uw}}{(1-\phi)P_u b_{uw} + P_t b_{tw} + N_0} < \kappa\right\} \\ &= \begin{cases} \Pr\left\{b_{uw} < \frac{(P_t b_{tw}+N_0)\kappa}{(\phi-[1-\phi]\kappa)P_u}\right\} & ,\kappa < \frac{\phi}{1-\phi} \\ 1 & ,\kappa \ge \frac{\phi}{1-\phi} \end{cases} \\ &= \begin{cases} \tilde{\Lambda}_w^d\left(B_{wd}, A_{wd}\right) & ,\kappa < \frac{\phi}{1-\phi} \\ 1 & ,\kappa \ge \frac{\phi}{1-\phi} \end{cases}\end{aligned} \tag{19}$$

where $l = \{c, d\}$, $B_{wd} = \frac{\kappa P_t}{\phi-(1-\phi)\kappa}$, $A_{wd} = \frac{B_{wd}N_0}{P_t}$ and

$$\tilde{\Lambda}_w^l\left(B_{wl}, A_{wl}\right) = \Pr\left\{b_{uw} < \frac{B_{wl}b_{tw} + A_{wl}}{P_u}\right\}, \tag{20}$$

which is deferred to Appendix B.

SOP for t_c. It is to evaluate the probability of WU failing to decode t_d (i.e., channel capacity that WU achieves for decoding t_d is smaller than E), or WU decoding t_d successfully but failing to decode t_c (i.e., channel capacity that WU achieves for decoding t_c is smaller than E):

$$\begin{aligned}\Lambda_w^c &= \Pr\left\{\log_2\left(\Psi_w^d+1\right) < E\right\} \\ &\quad + \Pr\left\{\log_2\left(\Psi_w^d+1\right) \ge E, \log_2\left(\Psi_w^c+1\right) < E\right\} \\ &= \Pr\left\{\Psi_w^d < \kappa\right\} + \Pr\left\{\Psi_w^d \ge \kappa, \Psi_w^c < \kappa\right\} \\ &= 1 - \Pr\left\{\Psi_w^d \ge \kappa, \Psi_w^c \ge \kappa\right\}.\end{aligned} \tag{21}$$

Substituting (11) and (12) into (21) yields (22) where $B_{wc} = \max\left(\frac{P_t\kappa}{\phi-\kappa(1-\phi)}, \frac{P_t\kappa}{1-\phi}\right)$ and $A_{wc} = \frac{B_{wc}}{P_t}N_0$.

$$\Lambda_w^c = 1 - \Pr\left\{\frac{\phi P_u b_{uw}}{(1-\phi) P_u b_{uw} + P_t b_{tw} + N_0} \geq \kappa, \frac{(1-\phi) P_u b_{uw}}{P_t b_{tw} + N_0} \geq \kappa\right\} = \begin{cases} \tilde{\Lambda}_w^c (B_{wc}, A_{wc}) & , \kappa < \frac{\phi}{1-\phi} \\ 1 & , \kappa \geq \frac{\phi}{1-\phi} \end{cases} \quad (22)$$

Comment: Equations (14), (17), (19), and (22) expose that {DU, CU, WU} completely fall in outage ($\Lambda_m^l = 1$, $m = \{d, c, w\}$) under certain circumstances. To be particular, a holistic outage occurs when E and ϕ meet $\kappa = 2^E - 1 \geq \frac{\phi}{1-\phi}$. Nevertheless, hindering such an occurrence is feasible by controlling E and ϕ to meet $\kappa < \frac{\phi}{1-\phi}$. This asks network designers to upper-limit the preset spectral efficiency E to meet $E < -\log_2(1-\phi)$ for hindering the holistic reliability outage at CU and DU whilst lower-limit E to satisfy $E > -\log_2(1-\phi)$ to induce the holistic outage at WU (equivalently, absolutely secured). Furthermore, (14), (17), (19), and (22) indicates that the reliability/security (namely, the desired REE/SEE or RST/SST or SOP/ROP) is accomplishable by controlling flexibly (ϕ, P_t, Q, φ, E).

3.4. SST/RST

NOFEwJ's throughput obeying delay constraints is derived explicitly from the analysis of the outage probability as

$$\Theta_m^l = E\left(1 - \Lambda_m^l\right), \quad (23)$$

where Θ_m^l represents the throughput of the device l whose message is decoded at device m. This implies that Θ_c^c and Θ_d^d are the RST of CU and DU, respectively, while Θ_w^c and Θ_w^d are the SST of CU and DU, respectively. Therefore, to achieve the desired RST/SST, it is necessary to appropriately configure and flexibly adjust the parameters (ϕ, P_t, Q, φ, E) within their feasible value range, as this set influences the quantity Λ_m^l, thereby affecting the RST/SST.

3.5. REE/SEE

REE and SEE are pivotal indicators used to quantify the efficiency of energy resource utilization in achieving the target transmission rate. Accordingly, REE and SEE are defined as

$$\Phi_{rel} = \frac{\Theta_d^d + \Theta_c^c}{P_t} \text{ and } \Phi_{sec} = \frac{\Theta_w^d + \Theta_w^c}{P_t}. \quad (24)$$

3.6. Performance limit

In the analysis of communication systems, studying the upper-bounded performance under large transmit power conditions helps researchers understand the behavior of the system when energy resources become abundant and interference power becomes unlimited. This analysis aids in determining the theoretical maximum performance that DU, CU, and WU can achieve in NOFEwJ, thereby providing insights into the system's capacity and limits. Indeed, as the transmit power of LT is large, i.e. $P_t \to \infty$, UT will accumulate infinite energy, resulting in $\tilde{P}_u \to \infty$. Therefore, $P_u \to P_{u\_\infty} = \frac{Q}{b_{ur}}$. Thus, the CDF and PDF of P_{u_∞} are calculated as

$$F_{P_{u\_\infty}}(z) = \Pr\left\{\frac{Q}{b_{ur}} < z\right\} = 1 - F_{b_{ur}}\left(\frac{Q}{z}\right), \quad (25)$$

and

$$f_{P_{u\_\infty}}(z) = \frac{Q}{z^2} f_{b_{ur}}\left(\frac{Q}{z}\right). \quad (26)$$

Consequently, NOFEwJ's ROP ($\Lambda_l^{l\_\infty}$) and SOP ($\Lambda_{\bar{w}}^{l\_\infty}$), respectively, can be distinctly derived as follows (the proof is similar to Appendices A and B):

$$\Lambda_l^{l\_\infty} = \begin{cases} \tilde{\Lambda}_l^{l\_\infty}(Z_l) & , \kappa < \frac{\phi}{1-\phi} \\ 1 & , \kappa \geq \frac{\phi}{1-\phi} \end{cases} \quad (27)$$

and

$$\Lambda_{\bar{w}}^{l\_\infty} = \begin{cases} \tilde{\Lambda}_{\bar{w}}^{l\_\infty}(B_{wl}, A_{wl}) & , \kappa < \frac{\phi}{1-\phi} \\ 1 & , \kappa \geq \frac{\phi}{1-\phi} \end{cases} \quad (28)$$

where

$$\begin{aligned} \tilde{\Lambda}_l^{l\_\infty}(a) &= \int_0^{\pi/2} F_{b_{ul}}\left(\frac{a}{\tan y}\right) f_{P_{u\_\infty}}(\tan y) \frac{dy}{\cos^2 y} \\ &= \frac{\pi^2}{4H} \sum_{i=1}^{H} \frac{\sqrt{1-\chi_i^2}}{\cos^2 \nu_i} F_{b_{ul}}\left(\frac{a}{\tan \nu_i}\right) f_{P_{u\_\infty}}(\tan \nu_i), \end{aligned} \quad (29)$$

and $\tilde{\Lambda}_{\bar{w}}^{l\_\infty}(B_{wl}, A_{wl})$ is expressed by (30) with $\chi_i = \cos\left(\frac{2i-1}{2H}\pi\right)$ and $\nu_i = \frac{\pi}{4}(\chi_i + 1)$.

4. Analytical Evaluation of OFEwJ

In OFEwJ, the message transmission process is divided into two equal phases, each lasting for half a second (assuming that the communication block is normalized to one second). During each phase, UT still operates with FD. More specifically, UT harvests energy from LT and uses it to transmit messages to either CU or DU. The transmit powers ($\tilde{P}_u$ and P_u) in this case remain the same as defined in (4) and (5). Accordingly, the received signal at LU is expressed as

$$m_l = k_{ul}\sqrt{P_u} t_l + \zeta_l. \quad (31)$$

$$\begin{aligned}\tilde{\Lambda}_w^{l_{-\infty}}(B_{wl}, A_{wl}) &= 1 - \int_0^{\pi/2} \frac{e^{-\frac{A_{wl}}{h_{uw}\tan y}} h_{uw}\tan y}{B_{wl}h_{tw}P_t + h_{uw}\tan y} f_{P_{u\_\infty}}(\tan y)\frac{dy}{\cos^2 y} \\ &= 1 - \frac{\pi^2}{4H}\sum_{i=1}^{H}\frac{\sqrt{1-\chi_i^2}}{\cos^2\nu_i}\left(\frac{e^{-\frac{A_{wl}}{h_{uw}\tan\nu_i}} h_{uw}\tan\nu_i}{B_{wl}h_{tw}P_t + h_{uw}\tan\nu_i}\right) f_{P_{u\_\infty}}(\tan\nu_i)\end{aligned} \tag{30}$$

The SINR for decoding t_l is obtained from (31) as

$$\bar{\Psi}_l^l = \frac{P_u b_{ul}}{N_0}. \tag{32}$$

The ROP at LU is given by

$$\bar{\Lambda}_l^l = \Pr\left\{\frac{1}{2}\log_2\left(1+\bar{\Psi}_l^l\right) \le E\right\} = \Pr\left\{\bar{\Psi}_l^l < \bar{\kappa}\right\}, \tag{33}$$

where $\bar{\kappa} = 2^{2E} - 1$.

Substituting (32) into (33) yields

$$\bar{\Lambda}_l^l = \Pr\left\{\frac{P_u b_{ul}}{N_0} < \bar{\kappa}\right\} = \Pr\left\{b_{ul} < \frac{N_0\bar{\kappa}}{P_u}\right\} = \tilde{\Lambda}_l(N_0\bar{\kappa}). \tag{34}$$

Analogously, WU observes the following signal:

$$m_{wl} = k_{uw}\sqrt{P_u}t_l + k_{tw}\sqrt{P_t}t_t + \zeta_w. \tag{35}$$

The SINR for decoding t_l is obtained from (35) as

$$\bar{\Psi}_w^l = \frac{P_u b_{uw}}{P_t b_{tw} + N_0}. \tag{36}$$

Accordingly, the ROP at WU is

$$\bar{\Lambda}_w^l = \Pr\left\{\frac{1}{2}\log_2\left(1+\bar{\Psi}_w^l\right) \le E\right\} = \Pr\left\{\bar{\Psi}_w^l < \bar{\kappa}\right\}. \tag{37}$$

Substituting (36) into (37) yields

$$\begin{aligned}\bar{\Lambda}_w^l &= \Pr\left\{\frac{P_u b_{uw}}{P_t b_{tw} + N_0} < \bar{\kappa}\right\} \\ &= \Pr\left\{b_{uw} < \frac{(P_t b_{tw} + N_0)\bar{\kappa}}{P_u}\right\} \\ &= \tilde{\Lambda}_w^l\left(\bar{B}_{wl}, \bar{A}_{wl}\right),\end{aligned} \tag{38}$$

where $\bar{B}_{wl} = \bar{\kappa}P_t$ and $\bar{A}_{wl} = \bar{\kappa}N_0$.

For OFEwJ, the RST/SST is obtained to be

$$\bar{\Theta}_m^l = E\left(1 - \bar{\Lambda}_m^l\right)/2, \tag{39}$$

and the REE and SEE are correspondingly computed to be $\bar{\Phi}_{rel} = \frac{\bar{\Theta}_d^d + \bar{\Theta}_c^c}{P_t}$ and $\bar{\Phi}_{sec} = \frac{\bar{\Theta}_w^d + \bar{\Theta}_w^c}{P_t}$.

5. Illustrative Results

This section provides an extensive performance evaluation of NOFEwJ under various scenarios, incorporating key parameters and a comparative analysis with the reference model, OFEwJ. The performance assessment is carried out using both analytical derivations ('The') and simulation methods ('Sim') to validate the reliability of the results. System parameters are selected to emulate realistic deployment scenarios, where user locations are randomly distributed across a two-dimensional spatial region. Here are default parameters: LT is located at (-10, 10), UT at (0, 0), LR at (60, 80), WU at (-20, -30), CU at (40, 0), and DU at (60, 10); the energy converting efficiency is $\varphi = 0.5$; the path loss decay is $\alpha = 2.8$; the self-interference power is $h_{uu} = -50$ dB; the required spectral efficiency is $E = 0.5$ bps/Hz; the power allocation factor is $\phi = 0.9$; the noise variance is $N_0 = -90$ dBm; the reference path loss $\beta = -10$ dB; and the transmission power of LT is $P_t = 20$ dBm.

The results presented in Fig. 2-6 illustrate a close match between 'Sim' and 'The', thence verifying the accuracy of the formulas developed in Section 3 and Section 4. This consistency reinforces the reliability of the proposed analysis and presents valuable understandings into the secrecy capability of NOFEwJ as compared with OFEwJ for numerous operating circumstances.

Fig. 2 compares the secrecy performance between the proposed NOFEwJ and the benchmarked OFEwJ by evaluating the throughput gap[3] with respect to (wrt) the transmission power of the licensed transmitter. Clearly, the secrecy capability of NOFEwJ reaches a saturation point as P_t increases, which aligns with the theoretical analysis presented earlier. Furthermore, the saturated throughput gap observed in NOFEwJ is approximately double that of its OFEwJ counterpart, underscoring the security advantage of the proposed model. It is also evident that as P_t increases, both

[3]Following the approaches in [3] and [32], the primary performance metric used to assess secrecy capability is the throughput gap, which has the same physical interpretation as the secrecy rate [36]. Specifically, the throughput gap is defined as $\left(\Theta_d^d + \Theta_c^c\right) - \left(\Theta_w^d + \Theta_w^c\right)$. A larger throughput gap indicates a higher level of security.

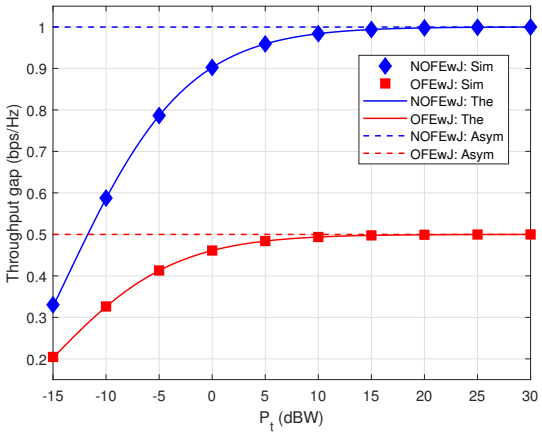

Figure 2. Throughput gap wrt P_t. "Asym" means Asymptote (i.e., throughput gap at high P_t)

systems exhibit improved performance, primarily due to the corresponding rise in harvested energy.

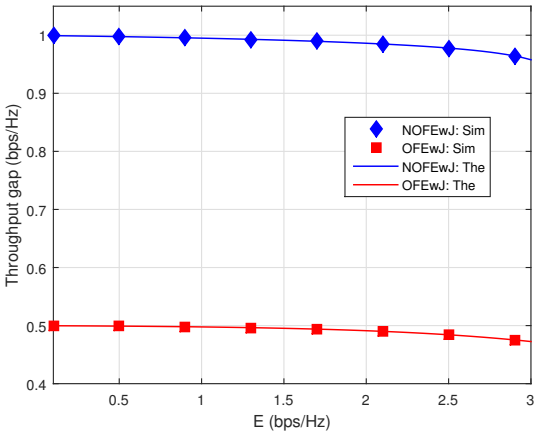

Figure 3. Throughput gap wrt E

Fig. 3 illustrates the throughput gap between the two systems under consideration when E fluctuates. Obviously, the proposed NOFEwJ significantly outperforms the benchmarked OFEwJ across the entire range of E, highlighting the remarkable benefit of jointly applying NOMA and FD communication, in contrast to using FD alone. Moreover, the secrecy performance deteriorates as E increases for both NOFEwJ and OFEwJ, as anticipated.

Fig. 4 reveals the effect of the power distribution coefficient ϕ on the throughput gaps of NOFEwJ and OFEwJ. Across the entire range of ϕ, NOFEwJ exhibits superior performance to OFEwJ, highlighting the efficacy of integrating FD and NOMA technologies. It is also observed that the secrecy capability of NOFEwJ is highly sensitive to variations in ϕ, whereas OFEwJ

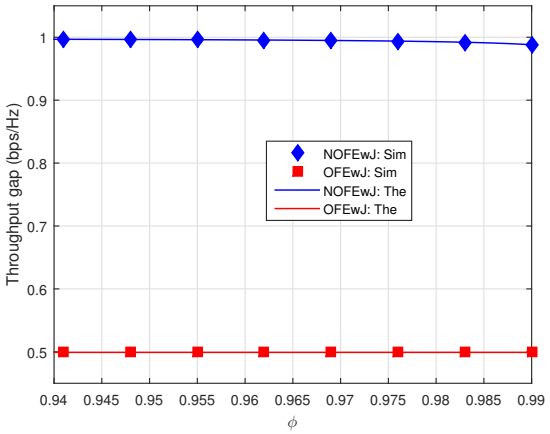

Figure 4. Throughput gap wrt ϕ

remains largely unaffected, which aligns with the inherent limitations of its orthogonal access structure.

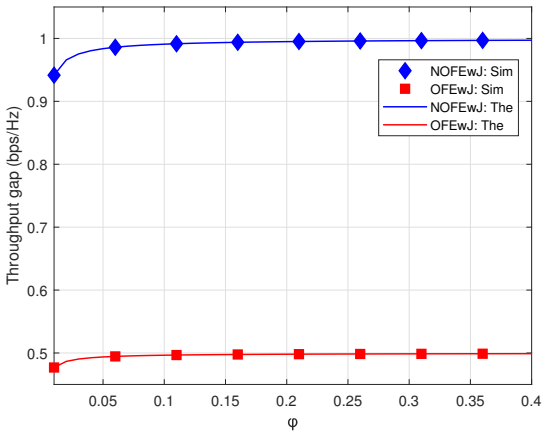

Figure 5. Throughput gap wrt φ

Fig. 5 presents the influence of φ on secrecy performance. The proposed NOFEwJ maintains a consistent advantage over OFEwJ for all values of φ, thereby reaffirming the efficacy of jointly deploying NOMA and FD in enhancing physical-layer security. Moreover, as φ increases - indicating greater energy harvesting capability - the secrecy performance of NOFEwJ improves markedly, while OFEwJ exhibits only a marginal gain, as theoretically anticipated.

Fig. 6 compares the secrecy performance of NOFEwJ with OFEwJ as a function of the maximum tolerable interference power Q at LR. Similarly, NOFEwJ consistently outperforms OFEwJ across the entire range of Q, validating the outstanding efficiency of combining FD and NOMA technologies compared to using FD alone. In addition, the secrecy capability of NOFEwJ and OFEwJ ameliorates with increasing Q due to higher tolerable interference at LR. Additionally, the secrecy

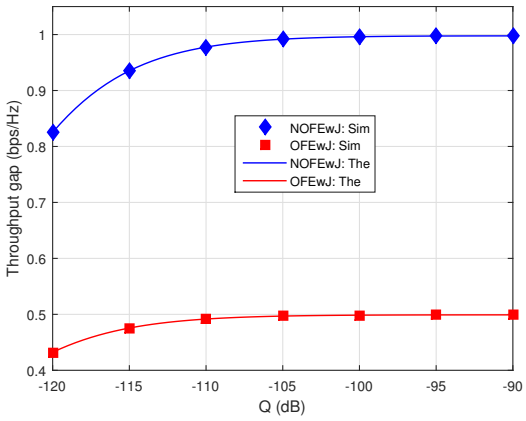

Figure 6. Throughput gap wrt Q

capability of NOFEwJ and OFEwJ saturates at high Q (e.g., $Q \geq -100$ dB), as expected owing to the power allocation in (5).

6. Conclusions

This research presents a secrecy analysis of NOMA CRNs with FD ES unlicensed transmitter under the exploitation of the licensed transmitter's interference as a jamming source for the improved security. By deriving explicit analytical expressions, the study enables a fast and efficient evaluation of key performance indicators like secrecy efficiency and throughput. Moreover, the comparative analysis with the benchmarked OFEwJ highlights the advantages of simultaneously integrating NOMA and FD transmission, as opposed to employing FD alone. This demonstrates the superior performance of NOFEwJ across various parameter configurations, thereby offering valuable insights for future research and practical implementations.

Appendix A: Derivation of $\tilde{\Lambda}_l(a)$

From (4), the CDF of $\tilde{P}_u$ is expressed as

$$\begin{aligned} F_{\tilde{P}_u}(z) &= \Pr\left\{\frac{\varphi b_{tu}}{1-\varphi b_{uu}} P_t \leq z\right\} \\ &= \int_0^{\frac{1}{\varphi}} F_{b_{tu}}\left(\frac{1-\varphi y}{P_t \varphi} z\right) f_{b_{uu}}(y)\, dy. \end{aligned} \tag{40}$$

Substituting (1) and (2) into (40) yields

$$\begin{aligned} F_{\tilde{P}_u}(z) &= \int_0^{\frac{1}{\varphi}} \left(1 - e^{-\frac{(1-\varphi y)z}{P_t \varphi h_{tu}}}\right) \frac{e^{-\frac{y}{h_{uu}}}}{h_{uu}} dy \\ &= 1 - N + \left(\frac{z}{H} - 1\right)^{-1} \left(e^{-Tz} - N\right), \end{aligned} \tag{41}$$

where $H = h_{tu} P_t / h_{uu}$, $T = \left(h_{tu} P_t \varphi\right)^{-1}$, and $N = e^{-(h_{uu}\varphi)^{-1}}$.

The PDF of $\tilde{P}_u$, $f_{\tilde{P}_u}(z)$, is obtained by differentiating $F_{\tilde{P}_u}(z)$ with respect to the variable z:

$$f_{\tilde{P}_u}(z) = H\left[\frac{N}{(z-H)^2} - \frac{e^{-Tz}}{(z-H)^2} - T\frac{e^{-Tz}}{z-H}\right]. \tag{42}$$

From (5), the CDF of P_u is given by

$$\begin{aligned} F_{P_u}(z) &= \Pr\left\{\tilde{P}_u < z, \tilde{P}_u < \frac{Q}{b_{ur}}\right\} \\ &\quad + \Pr\left\{\frac{Q}{b_{ur}} < z, \tilde{P}_u > \frac{Q}{b_{ur}}\right\} \\ &= \int_{\frac{Q}{z}}^{\infty} f_{b_{ur}}(x)\, dx + \int_0^{\frac{Q}{z}} F_{\tilde{P}_u}(z)\, f_{b_{ur}}(x)\, dx. \end{aligned} \tag{43}$$

Substituting (2) and (41) into (43) yields

$$\begin{aligned} F_{P_u}(z) &= \int_{\frac{Q}{z}}^{\infty} \frac{e^{-\frac{x}{h_{ur}}}}{h_{ur}} dx + F_{\tilde{P}_u}(z) \int_0^{\frac{Q}{z}} \frac{e^{-\frac{x}{h_{ur}}}}{h_{ur}} dx \\ &= 1 - \bar{F}_{\tilde{P}_u}(z) F_{b_{ur}}\left(\frac{Q}{z}\right). \end{aligned} \tag{44}$$

The PDF of P_u, $f_{P_u}(z)$, is obtained by differentiating $F_{P_u}(z)$ with respect to the variable z:

$$f_{P_u}(z) = f_{\tilde{P}_u}(z) F_{b_{ur}}\left(\frac{Q}{z}\right) + \frac{Q}{z^2} f_{b_{ur}}\left(\frac{Q}{z}\right) \bar{F}_{\tilde{P}_u}(z). \tag{45}$$

Equations (15) is rewritten as

$$\tilde{\Lambda}_l(a) = \int_0^{\infty} F_{b_{ul}}\left(\frac{a}{z}\right) f_{P_u}(z)\, dz. \tag{46}$$

By $z = \tan y$, (46) becomes

$$\tilde{\Lambda}_l(a) = \int_0^{\pi/2} F_{b_{ul}}\left(\frac{a}{\tan y}\right) f_{P_u}(\tan y) \frac{dy}{\cos^2 y}. \tag{47}$$

Applying Gauss-Chebyshev quadrature [38], we arrive at

$$\tilde{\Lambda}_l(a) = \frac{\pi^2}{4H} \sum_{i=1}^{H} \frac{\sqrt{1-\chi_i^2}}{\cos^2 \nu_i} F_{b_{ul}}\left(\frac{a}{\tan \nu_i}\right) f_{P_u}(\tan \nu_i). \tag{48}$$

Appendix B: Derivation of $\tilde{\Lambda}_w^l(B_{wl}, A_{wl})$

Equations (20) is rewritten as

$$\tilde{\Lambda}_w^l(B_{wl}, A_{wl}) = \Xi_{P_u}\left\{\hat{\Lambda}_w^l\right\}, \tag{49}$$

where

$$\hat{\Lambda}_w^l = \Xi_{b_{tw}} \left\{ F_{b_{uw}} \left(\frac{B_{wl} b_{tw} + A_{wl}}{P_u} \right) \right\}. \tag{50}$$

Substituting (1) and (2) into (50) yields

$$\begin{aligned} \hat{\Lambda}_w^l &= \int_0^\infty F_{b_{uw}} \left(\frac{B_{wl} x + A_{wl}}{P_u} \right) f_{b_{tw}}(x)\, dx \\ &= 1 - \frac{h_{uw} P_u}{B_{wl} h_{tw} + h_{uw} P_u} e^{-\frac{A_{wl}}{h_{uw} P_u}}. \end{aligned} \tag{51}$$

Substituting (51) into (49) yields

$$\tilde{\Lambda}_w^l (B_{wl}, A_{wl}) = 1 - \int_0^\infty \frac{h_{uw} x}{B_{wl} h_{tw} + h_{uw} x} e^{-\frac{A_{wl}}{h_{uw} x}} f_{P_u}(x)\, dx. \tag{52}$$

By $x = \tan y$, (52) becomes (53). Then, applying Gauss-Chebyshev quadrature, we arrive at (54).

$$\tilde{\Lambda}_w^l (B_{wl}, A_{wl}) = 1 - \int_0^{\pi/2} \frac{h_{uw} \tan y}{B_{wl} h_{tw} + h_{uw} \tan y} e^{-\frac{A_{wl}}{h_{uw} \tan y}} f_{P_u}(\tan y) \frac{dy}{\cos^2 y} \tag{53}$$

$$\tilde{\Lambda}_w^l (B_{wl}, A_{wl}) = 1 - \frac{\pi^2}{4H} \sum_{i=1}^{H} \frac{\sqrt{1 - \chi_i^2}}{\cos^2 \nu_i} \frac{f_{P_u}(\tan \nu_i)\, h_{uw} \tan \nu_i}{B_{wl} h_{tw} + h_{uw} \tan \nu_i} e^{-\frac{A_{wl}}{h_{uw} \tan \nu_i}} \tag{54}$$

References

[1] Ahn Y, Kim J, Kim S, Kim S, Shim B. Sensing and Computer Vision-Aided Mobility Management for 6G Millimeter and Terahertz Communication Systems [Journal Article]. IEEE Transactions on Communications. 2024;72(10):6044–6058.

[2] Shoaib M, Husnain G, Sayed N, Lim S. Unveiling the 5G Frontier: Navigating Challenges, Applications, and Measurements in Channel Models and Implementations [Journal Article]. IEEE Access. 2024;12:59533–59560.

[3] Le-Thanh T, Ho-Van K. Secure MIMO communication in energy harvesting-assisted NOMA Cognitive Radio Network with jamming under hardware impairment [Journal Article]. Physical Communication. 2024;66:102437. Available from: https://www.sciencedirect.com/science/article/pii/S1874490724001551.

[4] Le-Thanh T, Tran-Minh C, Ho-Van K. Underlay networks with nonorthogonal multiple access and energy harvesting: performance analysis [Journal Article]. Iranian Journal of Science and Technology, Transactions of Electrical Engineering. 2025;49(2):765–779. Available from: https://doi.org/10.1007/s40998-025-00803-8https://link.springer.com/article/10.1007/s40998-025-00803-8.

[5] Ho-Van K. IRS-enabled NOMA in energy scavenging underlay networks: Performance analysis [Journal Article]. International Journal of Communication Systems. 2025;38(3):e5987. Available from: https://doi.org/10.1002/dac.5987.

[6] Perera GS, Senanayake DY, Basnayake V, Jayakody DNK. Dynamic Spectrum Fusion: An Adaptive Learning Approach for Hybrid NOMA/OMA in Evolving Wireless Networks. In: 2024 4th International Conference on Advanced Research in Computing (ICARC);. p. 253–258.

[7] Zhang L, Yang H, Zhao Y, Hu J. Joint Port Selection and Beamforming Design for Fluid Antenna Assisted Integrated Data and Energy Transfer [Journal Article]. IEEE Wireless Communications Letters. 2024;13(7):1833–1837.

[8] Essa A, Almajali E, Mahmoud S, Amaya RE, Alja'Afreh SS, Ikram M. Wireless Power Transfer for Implantable Medical Devices: Impact of Implantable Antennas on Energy Harvesting [Journal Article]. IEEE Open Journal of Antennas and Propagation. 2024;5(3):739–758.

[9] Tyrovolas D, Mitsiou NA, Boufikos TG, Mekikis PV, Tegos SA, Diamantoulakis PD, et al. Energy-Aware Trajectory Optimization for UAV-Mounted RIS and Full-Duplex Relay [Journal Article]. IEEE Internet of Things Journal. 2024;11(13):24259–24272.

[10] Nayak VN, Gurrala KK. Secrecy Enhancement in AF Relaying Assisted SWIPT-NOMA via Power Optimization and Control-Jamming [Journal Article]. Wireless Personal Communications. 2024;135(1):431–450. Available from: https://doi.org/10.1007/s11277-024-11057-8.

[11] Doan TB, Nguyen TH. Enhancing covert communication in NOMA systems with joint security and covert design [Journal Article]. PLOS ONE. 2025;20(1):e0317289. Available from: https://doi.org/10.1371/journal.pone.0317289.

[12] Kang X, Qi N, Lv L, Boulogeorgos AAA, Tsiftsis TA, Liu H. Covert Communications in Active-IOS Aided Uplink NOMA Systems With Full-Duplex Receiver [Journal Article]. IEEE Transactions on Vehicular Technology. 2025;74(5):8419–8424.

[13] Reddy DK, Nayak VN, Rohan DBS, Sridhar PN. SOP ANALYSIS OF DF RELAYING-ENABLED SWIPT-NOMA NETWORK WITH DIFFERENT JAMMING CONDITIONS [Journal Article]. Telecommunications and Radio Engineering. 2025;84(3):51–63. Available from: https://www.dl.begellhouse.com/journals/0632a9d54950b268,6e1c139c0bb14bbc,2660ea395f03d002.html.

[14] Toan HV, Van QN, Hoang TM, Phan VD, Minh BV, Hiep PT, et al. Analysis of FD-NOMA Cognitive Relay System With Interference From Primary User Under Maximum Average Interference Power Constraint [Journal Article]. IEEE Access. 2021;9:161256–161268.

[15] Cao K, Wang B, Ding H, Lv L, Dong R, Cheng T, et al. Improving Physical Layer Security of Uplink NOMA via Energy Harvesting Jammers [Journal Article]. IEEE Transactions on Information Forensics and Security. 2021;16:786–799.

[16] Miridakis NI, Arzykulov S, Tsiftsis TA, Yang G, Nauryzbayev G. Green CR-NOMA: A New Interweave Energy Harvesting Transmission Scheme for Secondary Access. In: 2019 16th International Symposium on Wireless Communication Systems (ISWCS);. p. 571–576.

[17] Li F, Jiang H, Fan R, Tan P. Cognitive Non-Orthogonal Multiple Access With Energy Harvesting: An Optimal Resource Allocation Approach [Journal Article]. IEEE Transactions on Vehicular Technology. 2019;68(7):7080–7095.

[18] Singh CK, Singh V, Upadhyay PK, Lin M. Energy Harvesting in Overlay Cognitive NOMA Systems With Hardware Impairments [Journal Article]. IEEE Systems Journal. 2022;16(2):2648–2659.

[19] Shukla AK, Singh V, Upadhyay PK, Kumar A, Moualeu JM. Performance Analysis of Energy Harvesting-Assisted Overlay Cognitive NOMA Systems With Incremental Relaying [Journal Article]. IEEE Open Journal of the Communications Society. 2021;2:1558–1576.

[20] Bhowmick A, Roy SD, Kundu S. Throughput Maximization of a UAV Assisted CR Network With NOMA-Based Communication and Energy-Harvesting [Journal Article]. IEEE Transactions on Vehicular Technology. 2022;71(1):362–374.

[21] Vu TH, Nguyen TV, Kim S. Wireless Powered Cognitive NOMA-Based IoT Relay Networks: Performance Analysis and Deep Learning Evaluation [Journal Article]. IEEE Internet of Things Journal. 2022;9(5):3913–3929.

[22] Shi Z, Xie X, Lu H, Yang H, Cai J, Ding Z. Deep Reinforcement Learning-Based Multidimensional Resource Management for Energy Harvesting Cognitive NOMA Communications [Journal Article]. IEEE Transactions on Communications. 2022;70(5):3110–3125.

[23] Nguyen VS, Nguyen TH. Performance Analysis of Cognitive-Inspired Wireless Powered NOMA Systems With Joint Collaboration [Journal Article]. IEEE Access. 2023;11:51578–51589.
[24] Shukla AK, Yadav K, Upadhyay PK, Moualeu JM. Exploiting Deep Learning in the Performance Evaluation of EH-Based Coordinated Direct and Relay Transmission System With Cognitive NOMA [Journal Article]. IEEE Communications Letters. 2023;27(6):1501–1505.
[25] Yan P, Duan W, Ji X, Zhang G, Li B, Zou Y, et al. EH Cognitive Network With NOMA: Perspective on Impact of Passive and Active Eavesdropping [Journal Article]. IEEE Internet of Things Journal. 2024;11(3):5050–5062.
[26] Agrawal K, Flanagan MF, Prakriya S. NOMA With Battery-Assisted Energy Harvesting Full-Duplex Relay [Journal Article]. IEEE Transactions on Vehicular Technology. 2020;69(11):13952–13957.
[27] Guo C, Zhao L, Feng C, Ding Z, Wang HM. Secrecy Performance of NOMA Systems With Energy Harvesting and Full-Duplex Relaying [Journal Article]. IEEE Transactions on Vehicular Technology. 2020;69(10):12301–12305.
[28] Ma L, Li E, Yang Q. On the Performance of Full-Duplex Cooperative NOMA With Non-Linear EH [Journal Article]. IEEE Access. 2021;9:145968–145976.
[29] Agrawal K, Jee A, Makhanpuri U, Prakriya S. Performance of Full-Duplex Cooperative NOMA With Mode Switching and an EH Near User [Journal Article]. IEEE Networking Letters. 2023;5(4):284–288.
[30] Agrawal K, Prakriya S, Flanagan MF. TS-Based SWIPT in Full-Duplex Relayed NOMA With Intelligent Relay Battery Management [Journal Article]. IEEE Transactions on Communications. 2023;71(9):5137–5151.
[31] Zhou F, Chu Z, Sun H, Hu RQ, Hanzo L. Artificial Noise Aided Secure Cognitive Beamforming for Cooperative MISO-NOMA Using SWIPT [Journal Article]. IEEE Journal on Selected Areas in Communications. 2018;36(4):918–931.
[32] Le-Thanh T, Ho-Van K. Secured NOMA Full-Duplex Transmission With Energy Harvesting [Journal Article]. IEEE Access. 2024;12:91342–91356.
[33] Ho-Van K. Secure MIMO NOMA transmission with energy harvesting-aided full-duplex jammer under erroneous channel information [Journal Article]. Digital Signal Processing. 2024;151:104532. Available from: https://www.sciencedirect.com/science/article/pii/S105120042400157X.
[34] Le-Thanh T, Ho-Van K. Secure nonorthogonal multiple access with energy harvesting-assisted full-duplex receivers [Journal Article]. ETRI Journal. 2025. Available from: http://dx.doi.org/10.4218/etrij.2024-0335.
[35] Singh CK, Upadhyay PK. Overlay Cognitive IoT-Based Full-Duplex Relaying NOMA Systems With Hardware Imperfections [Journal Article]. IEEE Internet of Things Journal. 2022;9(9):6578–6596.
[36] Ho-Van K, Sofotasios PC, Muhaidat S, Cotton SL, Yoo SK, Brychkov YA, et al. Security Improvement for Energy Harvesting Based Overlay Cognitive Networks With Jamming-Assisted Full-Duplex Destinations [Journal Article]. IEEE Transactions on Vehicular Technology. 2021;70(11):12232–12237.
[37] Wang D, Rezaei F, Tellambura C. Performance Analysis and Resource Allocations for a WPCN With a New Nonlinear Energy Harvester Model [Journal Article]. IEEE Open Journal of the Communications Society. 2020;1:1403–1424.
[38] Abramowitz M, Stegun IA. Handbook of Mathematical Functions with formulas, graphs, and mathematical tables. Washington, D.C: U.S. Dept. of Commerce: U.S. G.P.O; 1972.